Computer Optics Vol. 1, No. 1, pp. 105–112, 1989
Printed in Great Britain

0955-355X/89 $10.00 + 0.00

STUDY OF THE WAVEFRONT AND ASTIGMATISM OF PLANAR STRIPE-GEOMETRY HETEROSTRUCTURE LASERS IN THE $\lambda = 780$–900 nm RANGE

M. A. MAN'KO, B. I. MAKHSUDOV and PHAM VAN HOI

Abstract—For planar stripe-geometry GaAlAs/GaAs heterostructure lasers, astigmatism, wavefronts and directivity diagrams of radiation are studied and their dependence on pumping current is investigated by means of a modified Michelson interferometer. Experimental data are compared with those calculated using a model with smooth variation of the complex dielectric permeability in the form of an Epstein layer.

INTRODUCTION

Wavefronts of light beams radiated by injection lasers possess astigmatism [1], which means that in order to obtain light beams having circular profiles cylindrical optics must be employed. On the other hand, in a videodisc readout the beam astigmatism may be utilized to provide automatic system focusing. Hence a precise quantitative measurement of the wavefront is necessary if it is desired to use injection lasers in read/write information systems.

A series of papers (see the list in [2]) have demonstrated the possibility of applying the theory of dielectric waveguides to active stripe-geometry waveguides, an example of which is the active region of a stripe-geometry heterostructure laser. It is known [3] that in the lasing regime the gain and the optical losses compensate one another globally but not locally, and that the local gain is basically concentrated in the active region, while losses are in the passive surrounding region and of course at the end mirrors. In view of this distribution of gain and loss the field suffers an additional decay in the transverse cross-section as one recedes from the active region. Taking into account the nonzero contribution of the imaginary part of the dielectric permeability $\mathrm{Im}\,\varepsilon$, the wavefront of the mode will not be plane: it lags behind in regions of absorption and has a bulge in the direction of propagation. Therefore, phase variations arise along a transverse axis, with consequent amplitude oscillations. The optical gain at the mode centre contributes to its strong localization, and the influence of the contribution of $\mathrm{Im}\,\varepsilon$ appears to be decisive for the mode profile and its characteristics (the so-called gain directivity effect). In planar stripe-geometry heterostructure lasers, without the lateral optical confinement imposed by the gain directivity effect in a plane parallel to the p–n boundary, the constriction of the light beam caustic corresponds to a virtual source, situated within the resonator at a distance Δz_0 from the end mirror, whereas in a plane perpendicular to the p–n boundary the constriction remains at the end mirror itself.

Recently an increasing number of papers have been devoted to studying wavefront shapes in injection lasers [4–11]. Thus [4–6] presented experimentally obtained beam parameters of light emitted by stripe-geometry heterojunction lasers, namely the wavefront curvature radius R and Δz_0. These parameters are required for designing focusing and collimating devices used as radiation sources in injection lasers. Interferometric techniques based on a modified Mach–Zender interferometer [4], a diffraction interferometer [5] or a Wollaston interferometer [6] were employed. Microscopic measurements of Δz_0 were carried out in [12] for a wide class of single-frequency injection lasers covering the 700–1300 nm range.

In this work (Section 1 below) we describe wavefront shape measurements in the principal cross-section of a laser beam as a function of pumping current in planar stripe-geometry heterojunction lasers without lateral optical confinement. Our interference technique is based on a modified Michelson interferometer and is similar to the one described in [10]. Section 2 presents the measured dependence of Δz_0 on the pumping current and on the width of the stripe contacts. We study the wavefront phase distribution in orthogonal directions as a function of the pumping current and the Watt–Ampère characteristics. The influence of nonlinearities in the Watt–Ampère characteristics on wavefront shapes, and of stripe contact width on wavefront curvature, are

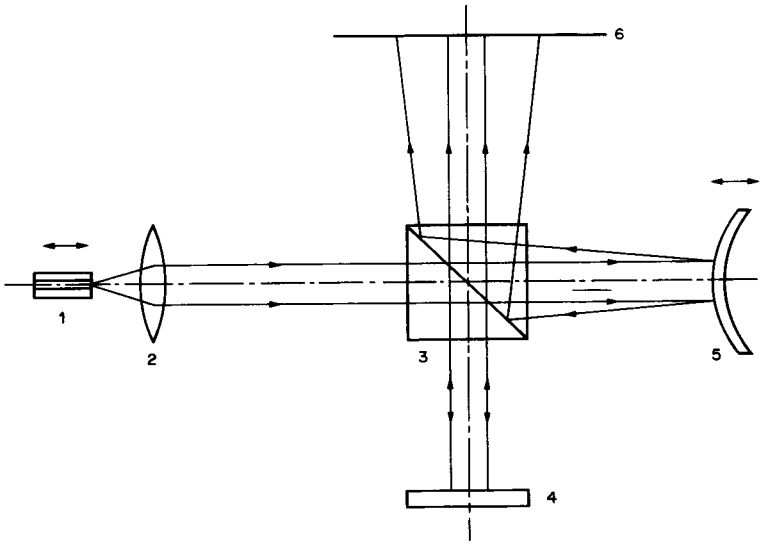

Fig. 1. Schematic diagram of apparatus to measure wavefronts in injection lasers. 1—Planar stripe geometry heterojunction laser; 2—objective; 3—beam splitter cube; 4—plane mirror; 5—spherical mirror; 6—electro-optical transducer or photodetector screen.

investigated. Section 3 compares experimental data with the predictions of a theoretical Epstein layer model based on a smooth variation of the complex dielectric permeability, which affords an estimate of active waveguide layer parameters affecting the directivity diagram.

1. EXPERIMENTAL METHOD

Figure 1 illustrates the experimental apparatus. Radiation from the heterojunction laser 1 was collimated by lens 2 and after being split by the cube 3 impinged on the plane mirror 4 in one of the arms of a Michelson interferometer, and on a convex spherical mirror 5 in the other arm. The axial portion of the beam expanded by the spherical mirror was chosen as reference, the visibility of the rings on the interferometer screen characterized the spatial coherence of the beam, and their geometry, i.e. the shape of the wavefront.

Displacing the laser along the optic axis (denoted by arrows in Fig. 1) results in a significant change in the interference pattern. Visual observation of changes in the interference pattern determined the position of the laser beam constriction in one plane relative to the constriction in the orthogonal plane, or relative to the end mirror of the laser diode. The constriction was measured by using the linear dependence between the displacement z of the diode and the cosine of the angle Δz between the asymptotes of the hyperbolic fringe on the interferometer screen [4]:

$$\cos \varphi = 1 + \Delta z/C, \tag{1}$$

where C is a constant.

The spacing z_0 between the constrictions was determined by the solutions of $\cos \varphi = \pm 1$, i.e. by the condition that the interference fringes formed a parallel system in two orthogonal directions. This technique allowed measurement of z_0 within ± 1 μm and of the phases to within $\pm 0.2\,\pi$.

We used planar stripe-geometry GaAlAs/GaAs heterojunction lasers without lateral optical confinement. The width of the active region varied from 0.15 to 0.35 μm, the resonator length from 160 to 240 μm, and the width of the stripe injection contacts from 8 to 16 μm. Operation was at room temperature, pumping 1.6 times threshold in Cw and 2.4 times threshold in the pulsed mode (pulse duration was 400 ns, repetition frequency 10^4 Hz). The range of measured wavelengths was 780–900 nm. Table 1 presents the characteristics of the samples studied.

Table 1. Characteristics of experimental samples with corresponding Δz_0

Heterojunction lasers	Threshold current J_{thr} (mA)	Width of stripe contacts (μm)	Wavelength λ (nm)	J/J_{thr}	Δz_0 (μm)
D.6.K	200	16	796.0	1 ÷ 1.4	23†
D.9.K	200	10	795.0	1 ÷ 1.5	25
D.13.K	170	12	788.8	1 ÷ 2.4	14 ÷ 22
D.9	225	16	799.7	1 ÷ 1.9	15
D.36	140	15	885.0	1 ÷ 2.0	15 ÷ 24‡
D.37	180	15	883.8	1 ÷ 1.6	18 ÷ 24‡
D.38	200	16	889.6	1 ÷ 1.5	15 ÷ 35‡
D.45	170	8	884.0	1 ÷ 1.6	9 ÷ 13

†In the kinked portion of the Watt–Ampère curve the interference pattern disappears.
‡The variation of Δz_0 with pumping current is nonmonotonic.

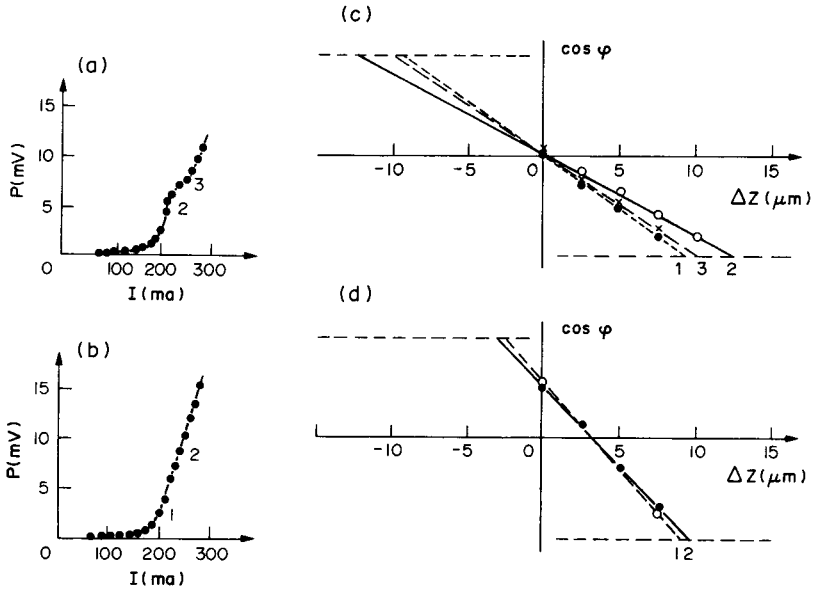

Fig. 2. Watt–Ampère characteristics (a, b) and dependence of cos φ on Δz(c, d) for various pumping currents whose values are indicated on the Watt–Ampère curves. (b) 1—200 mA, 2—220 mA, 3—240 mA; (c) 1—200 ma, 2—240 mA; for D.37 (a, b) and D.45 (c, d).

2. MEASUREMENT OF ASTIGMATISM AND WAVEFRONT SHAPE OF PLANAR, STRIPE-GEOMETRY GaAlAs/GaAs HETEROJUNCTION LASERS AS A FUNCTION OF PUMPING CURRENT

The Δz_0 values presented in Table 1 respond in a variety of ways to pumping-current variations: in a number of samples (e.g. D.9.K and D.9) Δz_0 stays the same, whereas in others (e.g. D.45 and D.13.K), monotonic increase of J_{thr} elicits a non-monotonic response Δz_0, in yet others (D.6.K) the interference pattern disappears at discontinuities in the Watt–Ampère characteristics.

The effect of pumping current on Δz_0 was investigated by performing measurements on a series of samples having different Watt–Ampère characteristics. Typical cases are illustrated in Fig. 2(a,b,c,d), Fig. 2(a) referring to step-like (sample D.37), 2(b) (D.45) to linear Watt–Ampère curves. In the first case the change in Δz (according to the foregoing Δz_0 is determined by the Δz of Eq. (1), as pumping current varies from 200 to 240 mA, is nonmonotonic (*cf.* Fig. 2a), unlike the case illustrated in Fig. 2(d), where Δz scarcely changes as the pumping current varies from 200 to 240 mA. The radiation wavefronts of sample D.37 at the various current values of continuous pumping plotted on the Watt–Ampère characteristic (Fig. 3a) are shown in Fig. 3(b) by the experimental points. The continuous curves are plotted from a theoretical model for the radiation phase distribution at the end mirror of the laser diode. The numerical values of parameters appended to the caption of Fig. 3 refers to these curves (*cf.* Section 3). It can be seen from Fig. 3 that the wavefront form varies as the pumping current increases. The observed wavefront variations at

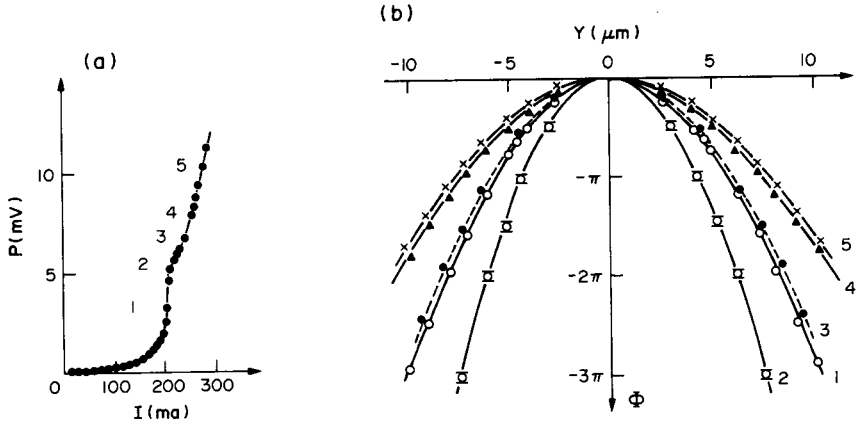

Fig. 3. Watt–Ampère characteristic (a), experimentally measured (points) and calculated wavefronts (b) of the D.37 laser for various pumping currents denoted by numbers on the Watt–Ampère curves: 1—20 mA, 2—220 mA, 3—2340 mA, 4—260 mA, 5—280 mA (continuous domain). Calculation was carried out with the following parameter values: 1—$\varepsilon_1 = \varepsilon_3 = 12.891 + i0.002$, $\varepsilon_2 = 12.786 - i0.003$, $l = 5.2$ μm; 2—$\varepsilon_1 = \varepsilon_3 = 12.891 + i0.005$, $\varepsilon_2 = 12.757 - i0.009$, $l = 3.2$ μm; 3—$\varepsilon_1 = \varepsilon_3 = 12.891 + i0.007$, $\varepsilon_2 = 12.801 - i0.009$, $l = 5.4$ μm; 4—$\varepsilon_1 = \varepsilon_3 = 12.891 + i0.007$, $\varepsilon_2 = 12.770 - i0.0095$, $l = 16$ μm; 5—$\varepsilon_1 = \varepsilon_3 = 12.891 + i0.007$, $\varepsilon_2 = 12.770 - i0.01$, $l = 16$ μm.

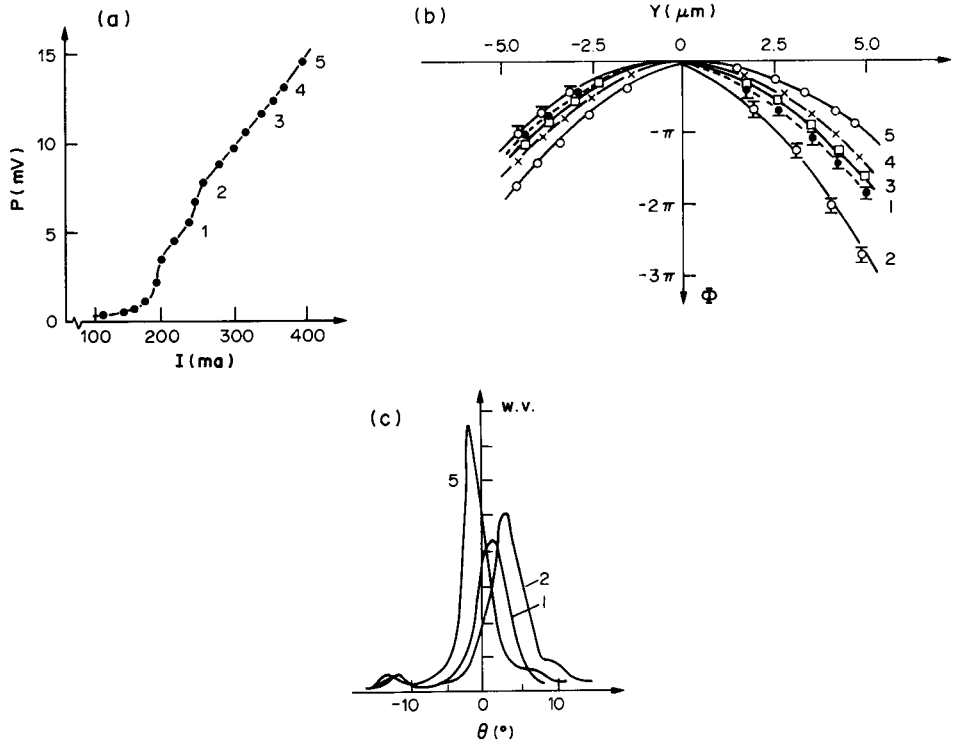

Fig. 4. Watt–Ampère characteristic (a), directivity diagram (b) and wavefront (c) of sample D.13.K for various values of pulsed pumping current: 1—240 mA, 2—260 mA, 3—320 mA, 4—360 mA, 5—400 mA (pulse length 400 nm, repetition rate 10 kHz).

higher excitation levels were obtained with pulsed pumping currents. Figure 4 shows the resulting behaviour in terms of the radiation distribution in the far zone (directivity diagram, Fig. 4b) and the wavefront (Fig. 4c) at the various pumping currents plotted in the Watt–Ampère curves (Fig. 4a) of the D.13.K laser diode. When the pumping current exceeds 1.5 times the threshold value, the wavefront becomes nonsymmetric. The asymmetry is connected with changes in the radiation intensity distribution in the near and far zones, and depends on the form of the Watt–Ampère

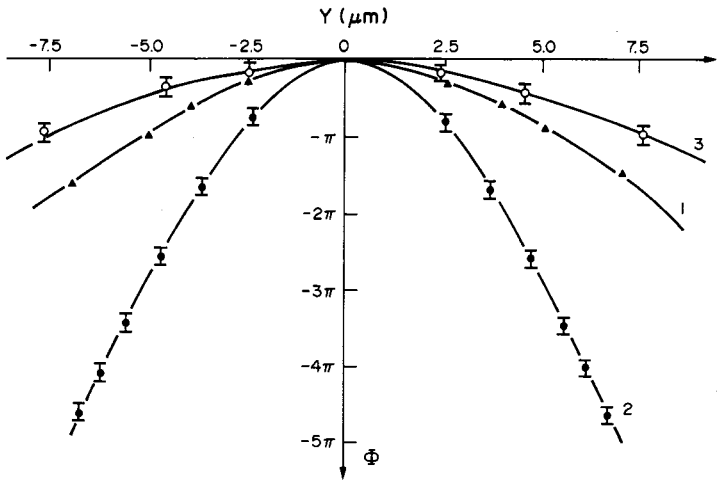

Fig. 5. Experimental measurements (points) and calculated phase distribution of the electromagnetics field at the end mirrors of samples D.6.K(1) D.37(2) and D.45(3), for pumping currents 10% in excess of threshold. Calculation was performed with the following parameter values: 1—$\varepsilon_1 = \varepsilon_3 = 12.891 + i0.001$, $\varepsilon_2 = 12.880 - i0.002$, $l = 4.7\ \mu m$, $\lambda = 800$ nm, $\Gamma_0 = 0.8$; 2—$\varepsilon_1 = \varepsilon_3 = 12.891 + i0.002$, $\varepsilon_2 = 12.786 - i0.003$, $l = 5.2\ \mu m$, $\lambda = 900$ nm, $\Gamma_0 = 0.8$; 3—$\varepsilon_1 = \varepsilon_3 = 12.891 + i0.003$, $\varepsilon_2 = 12.867 - i0.008$, $l = 1.5\ \mu m$, $\lambda = 900$ nm, $\Gamma_0 = 0.8$.

characteristics (the deviations from the optic axis are different for samples with linear and nonlinear Watt–Ampère curves).

Two series of samples possessing contact widths of 8 and 16 μm were used to investigate the effect of stripe contact width on the wavefront shape. The results are shown in Fig. 5, the points corresponding to experimental measurements for samples D.6.K, D.45 and D.37 at pumping currents 10% above threshold values. The continuous curve corresponds to the computed phase distribution of the electromagnetic field at the end mirrors, using the parameters in the caption to Fig. 5.

3. COMPARISON OF EXPERIMENTAL DATA WITH THEORETICAL LASER MODEL EMPLOYING AN EPSTEIN LAYER FOR A SMOOTHLY VARYING COMPLEX DIELECTRIC PERMEABILITY

The field distribution in the active region of a heterojunction laser is described by a Schroedinger type equation in which the dielectric permeability plays the role of the potential energy (*cf.* for example, [13]). For planar stripe-geometry heterojunction lasers without lateral optical confinement an acceptable model distribution for $\varepsilon(y)$ across the active region is provided by the Epstein layer [14], which is the analogue of the Eckart potential in quantum mechanics [14]. The Epstein layer profile for the dielectric permeability along the y axis is

$$\varepsilon(y) = (\varepsilon_3 - \varepsilon_1)\frac{\exp y/l}{1 + \exp y/l} + 2(2\varepsilon_2 - \varepsilon_1 - \varepsilon_3)\frac{\exp y/l}{(1 + \exp y/l)^2}, \tag{2}$$

where $\varepsilon_1 = \varepsilon(-\infty)$, $\varepsilon_2 = \varepsilon(0)$, $\varepsilon_3 = \varepsilon(\infty)$ and l is the layer width parameter, used in [2, 8–11, 16–17, 18–20].

If the distribution is symmetric ($\varepsilon_1 = \varepsilon_3 = \varepsilon_0$) Eq. (2) becomes

$$\varepsilon(y) = 4(\varepsilon_2 - \varepsilon_0)\frac{\exp y/l}{(1 + \exp y/l)^2} = \frac{\varepsilon_3 - \varepsilon_0}{\mathrm{ch}^2\, y/2l}. \tag{3}$$

A list of references employing a symmetric layer may be found in [18].

Following [21, 22] we shall write the solution of the wave equation when $\varepsilon(y)$ is given by (2) as follows:

$$Y_0(y) = \frac{\exp a_0 y/2l}{(\mathrm{ch}\, y/2l)^s} \qquad \text{for} \quad n = 0, \tag{4}$$

$$Y_1(y) = \frac{(\exp a_0 y/2l)(a_1 - \operatorname{sth} y/2l)}{(\operatorname{ch} y = 2l)^{s-1}} \qquad \text{for} \quad n = 1. \tag{5}$$

Two quantities were introduced in (4) and (5), the width parameter s and the asymmetry parameter a_n [2, 8, 10, 20, 21]:

$$s = \tfrac{1}{2}\{-1 \pm [1 + 8(2\varepsilon_2 - \varepsilon_1 - \varepsilon_3)k_0^2\Gamma_0 l^2]^{1/2}\}, \tag{6}$$

$$a_n = k_0^2\Gamma_0 l^2(\varepsilon_3 - \varepsilon_1)/(s - n), \tag{7}$$

where $\Gamma_0 = \int_{-d/2}^{d/2} |X(x)|^2\,dx / \int_{-\infty}^{\infty} |X(x)|^2\,dx$ is the optical confinement parameter along the x-axis, d is the heterojunction laser active region's width, $k_0 = 2\pi/\lambda$, and λ is the radiation wavelength. When the distribution is symmetric $a_n = 0$. Since the dielectric permeability is complex, $\varepsilon = \varepsilon' + i\varepsilon''$, s and a_n are also complex, $s = s' + is''$, $a_n = a_n' + ia_n''$. The phase of the electromagnetic field in the near zone (at the end mirror) for the fundamental $n = 0$ mode may be written in the form

$$\Phi = -s'' \ln(\operatorname{ch} y/2l) + a_0'' y/2l. \tag{8}$$

The field intensity distribution in the far zone (directivity diagram) can be determined in the usual manner in terms of the near zone pattern (*cf.* for example, [19, 22]).

We chose a set of values for s, a_0 and l in (8) so as to satisfy the experimentally observed wavefronts of the D.37 (*cf.* Fig. 4a,b) and D.6.K, D.45 (Fig. 5) lasers. Good agreement was obtained between the experimental data and curves calculated with the active waveguide parameter values listed in the captions to Figs 3(a,b) and 5. Note that for pumping currents corresponding to the nonlinear region of the Watt–Ampère curve an anomalous change in the wavefront curvature is observed. If one assumes this to be associated with a decrease in the waveguiding properties of the laser's active region, then for the appropriate set of dielectric parameters ($\varepsilon_1 = \varepsilon_3$ and ε_2, a symmetric active waveguide) a satisfactory agreement may be achieved between the calculated and experimental curves.

Let us now proceed to the inverse problem, and try to estimate the complex permeability in the active region, $\varepsilon = \varepsilon' + i\varepsilon''$, from data on wavefronts and on the amplitude of the electromagnetic field at the end mirror of the heterojunction laser. To do this, we use the results of [21, 22] from which we quote the following $n = 0$ mode relations:

$$s' = -\frac{1}{2} + \frac{1}{2\sqrt{2}}\{1 + 8k_0^2\Gamma_0 l^2\delta\varepsilon' + 16k_0^4\Gamma_0^2 l^4(\delta\varepsilon'^2 + \delta\varepsilon''^2)]^{1/2} + 1 + 4k_0^2\Gamma_0 l^2\delta\varepsilon'\}^{1/2}, \tag{9}$$

$$s'' = \frac{1}{2\sqrt{2}}\{[1 + 8k_0^2\Gamma_0 l^2\delta\varepsilon' + 16k_0^4\Gamma_0^2 l^4(\delta\varepsilon'^2 + \delta\varepsilon''^2)]^{1/2} - 1 - 4k_0^2\Gamma_0 l^2\delta\varepsilon'\}^{1/2}, \tag{10}$$

$$a_0' = \frac{k_0^2\Gamma_0 l^2}{s'^2 + s''^2}[s'(\varepsilon_3' - \varepsilon_1') + s''(\varepsilon_3'' - \varepsilon_1'')], \tag{11}$$

$$a_0'' = \frac{k_0^2\Gamma_0 l^2}{s'^2 + s''^2}[s'(\varepsilon_3'' - \varepsilon_1'') - s''(\varepsilon_3' - \varepsilon_1')], \tag{12}$$

where $\delta\varepsilon' = 2(2\varepsilon_2' - \varepsilon_1' - \varepsilon_3')$, $\delta\varepsilon'' = 2(2\varepsilon_2'' - \varepsilon_1'' - \varepsilon_3'')$.

Wavefront measurement provides an estimate for s'' and a_0'', while near-field patterns give s' and a_0'. Nonmonotonic variations of the active waveguide parameters s and a_n, and of the complex permeability $\varepsilon = \varepsilon' + i\varepsilon''$, originating in kinks and nonlinearities in the Watt–Ampère characteristics, give rise to anomalous changes in the wavefront curvature responsible for the nonmonotonic near and far-field pattern changes. Table 2 presents the experimentally obtained values of the parameters

Table 2. Experimental values of l, s'' and computed values of $\delta\varepsilon'$, $\delta\varepsilon''$ for the D.37 heterojunction laser

J (mA)	200	220	240	260	280
l (μm)	5.5	3.2	5.4	16	16
s''	−3.5	−2.29	−3.1	−11.26	−11.26
$\delta\varepsilon''$	−0.019	−0.056	−0.064	−0.066	−0.066
$\delta\varepsilon'$	−0.413	−0.535	−0.335	−0.494	−0.494

Table 3. Experimental values of l, s'', a_0'', and computed values of $\varepsilon_3' - \varepsilon_1''$, $\varepsilon_3'' - \varepsilon_1''$ for the D.13.K heterojunction laser

J (mA)	240	260	320	360	400
l (μm)	1	0.78	1.4	2.8	0.75
s''	−0.41	−0.39	−0.60	−1.79	−0.24
a_0''	−0.1	−0.16	−0.08	0	0.06
$\varepsilon_3' - \varepsilon_1'$	0.088	0.227	0.038	−0.00006	−0.1094
$\varepsilon_3'' - \varepsilon_1''$	0.001	0.003	0.0007	0.0002	−0.0007

l and s'', and the computed values of $\delta\varepsilon'$ and $\delta\varepsilon''$ for the D.37 heterojunction laser, whose wavefront variation with pumping current is shown in Fig. 3(b).

For the nonsymmetrical distribution $\varepsilon(y)$ in (2) we analyse the behaviour of the D.13.K heterojunction laser whose wavefront variation with pumping current is shown in Fig. 5(c). Table 3 gives the experimentally determined parameters l, s'' and a_0'', as well as the calculated values of $\varepsilon_3' - \varepsilon_1'$ and $\varepsilon_3'' - \varepsilon_1''$. We see that the asymmetry parameter a_0'' changes sign from negative to positive values, going through zero for pumping current values in excess of 1.5 times the threshold value. Let us try to calculate the complex permeabilities ε_1, ε_2, ε_3, by using the experimentally plotted wavefront of the D.13.K heterojunction laser (curve 1 in Fig. 4c) and results from our previous work [18, 19]. Following [20], we calculated in [21, 22] $\varepsilon_3' = 12.891$, and $\varepsilon_3'' = 0.0054$, while the present work gives us the quantities $\varepsilon'' = 0.41$, $\varepsilon_3' - \varepsilon_1' = 0.088$, and $\varepsilon_3'' - \varepsilon_1'' = 0.001$. Hence, we obtain $\varepsilon_1 = 12.803 + i0.0044$, $\varepsilon_2 = 12.743 - i0.006$, and $\varepsilon_3 = 12.891 + i0.0054$.

CONCLUSION

The comparison of the experimentally measured phase distribution at the exit mirror with the theoretical model calculation based on the Epstein layer, carried out in Section 3, has vindicated the utility of this model. Within this model one may vary the width of the active strip layer for a given permeability profile, take into account the dielectric asymmetry of the structure, as well as noncoincidence of the gain and refractive index maxima, and finally, allow for the negative contribution to the real part of the complex permeability due to the excess current carriers. The experimental measurements and the theoretical analysis of wavefronts of plane stripe-geometry heterojunction GaAlAs/GaAs lasers have led us to conclude that the wavefront change is closely connected with nonlinearities (kinks) in the Watt–Ampère curves; that the radiation directivity diagram is determined by the active layer's complex permeability profile—whose asymmetry grows with the pumping current; and that small fluctuations in the dielectric permeability of the activity layer give rise to significant changes in the shape of the wavefront.

Acknowledgements—The authors thank P. G. Eliseev and G. T. Mikaelyan for useful remarks.

REFERENCES

1. D. D. Cook and F. R. Nash. Gain-induced guiding and astigmatic output beam of GaAs-laser. *J. appl. Phys.* **46**, 1660–1672 (1975).
2. M. A. Man'ko and G. T. Mikaelyan. Modes and their transformation in active semiconducting waveguides. In: *Nonlinear Optics of Semiconducting Lasers*. Nauka, Moscow. *Trans. FIAN* **166**, 125–154 (1986).
3. P. G. Eliseev. *Introduction to the Physics of Injection Lasers*. Nauka, Moscow (1983).
4. K. Tatsumo and A. Arimoto. Measurement and analysis of diode laser wavefronts. *Appl. Opt.* **20**, 3520–3525 (1981).
5. L. Arquie. Semiconductor laser wavefronts. *Proc. Eur. Conf. Opt. Commun.*, Cannes, France, pp. 183–186 (1982).
6. D. C. Van Eck. Wavefront measurement on semiconductor laser. *IEEE J. Quantum Electron.* **QE-19**, 966–968 (1983).
7. D. W. Kunts. Specifying laser diodes optics. *Laser Focus* **20**, 44–55 (1983).
8. M. A. Man'ko, B. I. Makhsudov, G. T. Mikaelyan *et al.* Measurement and analysis of planar stripe-geometry GaAlAs/GaAs heterojunction laser wavefronts and their variation with pumping current. *IEE Proc. pt. J., Optoelectronics* **132**, 64–68 (1985).
9. M. A. Man'ko, B. I. Makhsudov and Pham Van Hoi. Study of wavefronts and astigmatism in planar, stripe-geometry heterojunction lasers with $\lambda = 7800$–9000 Å. Proc. Second Int. Conf. on Radiooptics, Tbilisi. (June 1985).
10. M. A. Man'ko, B. I. Makhmudov and Pham Van Hoi. Study of wavefronts in planar stripe-geometry GaAlAs/GaAs heterojunction lasers. In: *Nonlinear Optics of Semiconducting Lasers*. Nauka, Moscow. *Trans. FIAN* **166**, 155–165 (1986).
11. M. A. Man'ko and Pham Van Hoi. Astigmatism and wavefront of stripe-geometry heterojunction lasers. *Abstr. 5th Int. Conf. Lasers and their Applications*, Dresden, p. 100 (1985).
12. T. P. Lee, C. A. Burrus, D. Marcuse *et al.* Measurement of beam parameters of index-guided and gain-guided single-frequency InGaAsP injection lasers. *Electron. Lett.* **18**, 902–904 (1982).

13. T. L. Paoli. Waveguiding in stripe-geometry injection lasers. *Appl. Opt.* **23**, 94–99 (1984).
14. P. S. Epstein. Reflection of waves in an inhomogeneous absorbing media. *Proc. Natn. Acad. Sci.* **16**, 627–637 (1930).
15. Ph. M. Morse and H. Feshbach. *Methods of Theoretical Physics*, Vol. II. McGraw-Hill, London (1960).
16. W. Streifer, R. D. Burnham and D. R. Scifres. Symmetrical and asymmetrical waveguiding in very narrow conducting stripe lasers. *IEEE J. Quantum Electron.* **QE-15**, 136–141 (1979).
17. P. G. Eliseev and M. Osinskii. Application of the Epstein dielectric model to the description of modes in planar stripe-geometry heterojunction lasers. *Kvantovaya Elektronika* **7**, 1407 (1980).
18. T. Dziewiecka and M. Osinski. Generalized Epstein model of stripe-geometry injection lasers. *Appl. Opt.* **23**, 94–99 (1984).
19. P. A. Kirkby and G. H. B. Thompson. The effect of double-heterojunction waveguide parameters in the far field emission patterns of laser. *Optoelectronics* **4**, 323–324 (1972).
20. H. C. Casey Jr, D. D. Sell and M. B. Panish. Refractive index of $Al_xGa_{1-x}As$ between 1.2 and 1.8 eV. *Appl. Phys. Lett.* **24**, 63–65 (1974).
21. A. P. Bogatov, P. G. Eliseev, M. A. Man'ko *et al.* Model for stripe-geometry heterojunction laser including complex dielectric constant nonuniformities along the resonator. Preprint *FIAN SSSR* No. 101. Moscow (1981).
22. P. G. Eliseev, M. A. Man'ko and G. T. Mikaelyan. Model for injection laser with smoothly varying dielectric constant along the p–n boundary. In: *Injection Lasers*. Nauka, Moscow. *Trans. FIAN* **141**, 119–125 (1983).